

# Near Equipartition Magnetic Fields Measured in the Cool Cores of Galaxy Clusters

Ido Reiss<sup>1,2,\*</sup> and Uri Keshet<sup>1</sup>

<sup>1</sup>*Physics Department, Ben-Gurion University of the Negev, POB 653, Be'er-Sheva 84105, Israel*

<sup>2</sup>*Physics Department, Nuclear Research Center Negev, POB 9001, Be'er-Sheva 84190, Israel*

(Dated: August 2, 2012)

Tangential discontinuities, seen as X-ray edges known as cold fronts (CFs), are ubiquitous in cool-core galaxy clusters. We analyze all 18 deprojected CF thermal profiles found in the literature, including three new CFs we identify (in clusters A2204 and 2A0335). We discover small but significant thermal pressure drops below all non-merger CFs, and argue that they arise from strong, near-equipartition (10–20%) magnetic fields below and parallel to the discontinuity. Such magnetization can stabilize the CF against Kelvin-Helmholtz instabilities, and explain the connection between CFs and radio minihalos.

In the past decade, high resolution X-ray observations have revealed an abundance of density and temperature discontinuities known as cold fronts (CFs). They are broadly classified as cool-core CFs and merger CFs (for a review, see [1]); a third, putative class of shock-collision induced CFs [2], has not yet been observed. Here we focus exclusively on the first, cool-core, type of CFs.

Core CFs are observed in most of the otherwise relaxed, cool-core clusters (CCs) [3], in distances up to  $\sim 400$  kpc from the center. They are usually nearly concentric or spiral, and multiple CFs are often observed in the same cluster. The temperature contrast across such a CF is  $T_o/T_i \sim 2$  [4], where inside/outside subscripts  $i/o$  refer to regions closer to/farther from the cluster center, or equivalently below/above the CF. The plasma beneath the CF is typically denser, colder, much lower in entropy, and higher in metallicity, than the plasma above it.

Such CFs are thought to be a quasi-spiral tangential discontinuity surfaces seen in projection [5, 6]. They may reflect large-scale “sloshing” oscillations of the intracluster medium (ICM), driven by mergers [7], possibly involving only a dark matter subhalo [5, 8], or feedback from the central active galactic nucleus (AGN) in the form of weak shocks or acoustic waves displacing cold central plasma [9, 10]. They were also proposed to be the signature of long-lived spiral bulk flows underlying cool cores, sustained for example by AGN bubbles [6].

Deprojected thermal profiles across core CFs reveal the presence of fast, nearly sonic flows beneath, and tangential shear layers extending below, the CFs [11]. Such shear can produce the near-equipartition magnetic fields needed to stabilize the CF against Kelvin-Helmholtz instabilities (KHI),  $\eta_B \equiv P_B/P_{th} \equiv B^2/8\pi P_{th} = 10\text{--}20\%$  [11]. Here,  $B$  is the magnetic amplitude, and equipartition is defined as equal magnetic and thermal pressures,  $P_B = P_{th}$ . Such shear layers and magnetization levels were reproduced in CC sloshing simulations [12].

There is circumstantial evidence for strong magnetic fields along and below CFs. The thinness of the emission discontinuity, which is much narrower than the Coulomb mean free path, requires a magnetic suppression of transport across the CF [13]. The CF–radio minihalo connec-

tion ([14]; see also [15, 16]), in particular when combined with the correlation between the radio and X-ray brightness of mini-halos, suggests strong magnetization below CFs, significantly exceeding the cosmic microwave background equivalent  $\sim 3 \mu\text{G}$  [17].

Previous measurements of core magnetic fields [18–21] produced conflicting results, and are not particularly sensitive to the CF region. In this *letter* we report the discovery and direct measurement of a thermal pressure  $P_{th}$  discontinuity across core CFs. We interpret this as a discontinuous jump in nonthermal pressure  $P_{nt}$  below the CF, and argue that it must be predominantly magnetic. We assume a Hubble constant of  $H = 70 \text{ km s}^{-1} \text{ Mpc}^{-1}$ , and a 0.23 He mass fraction. Error bars represent  $1\sigma$  confidence levels.

*Core CFs do show a thermal pressure discontinuity.*—Unlike merger CFs, core CFs were so far thought to involve no change in thermal pressure (*i.e.* appear thermally isobaric; [1] and references therein). To critically examine this, we analyze the thermal profiles near core CFs, and derive the pressure on both sides of the CF.

We extract all the thermal profiles across core CFs in the literature, and select only profiles that have been deprojected along the line of sight. There are 15 such CFs from 10 CCs, in which  $P_{th}$  can be estimated on both sides of the CF. We compute  $P_{th}$  as the product of the deprojected particle number density and temperature, assuming a single-phase ideal gas. (Deviations from this assumption are discussed towards the end.) Some  $P_{th}(r)$  profiles are illustrated in Figure 3.

In Figure 1 we present the ratio  $\xi \equiv P_i/P_o$  between  $P_{th}$  just below the CF ( $P_i$ ) and  $P_{th}$  just above the CF ( $P_o$ ), for all CFs, as a function of the CF radius  $r_{cf}$  normalized by  $R_{500}$ . The values of  $R_{500}$ , the radius enclosing a mean density 500 times the critical density of the Universe, are taken from Ref. [22]. Literature references for the CF data are provided in the caption.

We first compute  $P_i$  and  $P_o$  assuming a radial power-law behavior on each side of the CF, estimated from the two nearest data points. In the three cases where only one temperature data point exists below the CF (the two CFs in RXJ1347.5 and the inner CF in A1644, marked

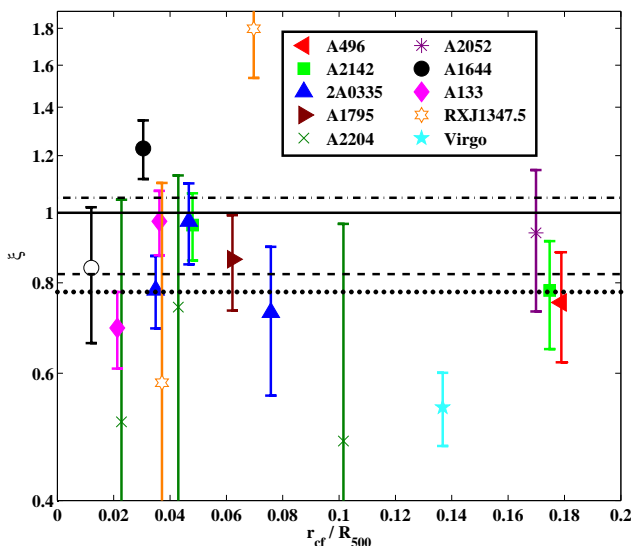


FIG. 1: The deprojected thermal pressure ratio  $\xi = P_i/P_o$ , plotted against the normalized radius  $r/R_{500}$ , for all core CFs. The solid line corresponds to thermally isobaric,  $\xi = 1$  transitions. Horizontal lines show the averages of all CFs (dotted line), of our final CF sample (dashed, Eq. (1)), and of the fictitious sample (dot-dashed); see text. An isothermal profile is assumed for CFs marked by empty symbols. Data: Ref. [25] for A496, Ref. [26] for A2142, Ref. [23] for 2A0335, Ref. [7] for A1795, Ref. [24] for A2204, Ref. [27] for A2052, Ref. [28] for A1644, Ref. [29] for A133, Ref. [30] for RXJ1347.5, and Ref. [31] for Virgo.

by empty symbols in Figure 1), we assume an isothermal temperature profile. We also identify three new CFs, seen coincidentally in the emission, temperature, and sometimes also metallicity: two in the Southwest sector of 2A0335 [23], at radii  $\sim 28$  and  $\sim 62$  kpc, and one in the West sector of A2204 [24], at  $r_{cf} \simeq 127$  kpc. These CFs are shown as dashed rectangles in Figure 3.

Confidence levels are estimated by error propagating the quoted uncertainties in the temperature and density data, assumed for simplicity to be statistical, normally distributed [49], and uncorrelated. The resulting error is dominated by the uncertainty in the temperature bin just above the CF. Our error estimate is conservative, yielding high uncertainties in the inferred pressure jumps. A more realistic estimate, using the covariance matrix between points above and below the CF, should yield the same nominal points with a reduced uncertainty.

All CFs, except two unusual cases discussed below, show  $\xi < 1$ , suggesting a  $P_{th}$  deficit below the CF. The statistical significance per CF is modest (between  $0.3\sigma$  and  $3.6\sigma$ , except Virgo with  $7.3\sigma$ ), but the similar trend among CFs renders this result robust. The mean result for all CFs is  $\bar{\xi}_{all} = 0.78 \pm 0.03$ . The two unusual CFs with  $\xi > 1$  are the outer CFs in A1644 and RXJ1347.5, both of which are known to be undergoing a merger. This suggests that these CFs were disrupted by the merger;

excluding them from the analysis leaves a non-disrupted CF average  $\bar{\xi} = 0.74 \pm 0.03$ . The CF sector in Virgo is narrow and shows evidence of density substructure, as seen in Figures 2 and 3, so it is henceforth excluded as well. The mean result for the remaining 15 CFs is

$$\bar{\xi} = 0.82 \pm 0.04. \quad (1)$$

We conclude that  $\bar{\xi} \simeq 0.8$ , with a large dispersion among CFs, is significantly smaller than unity.

In order to show that the result is not an artifact of the deprojection method, we apply the same analysis method to the projected radial profiles. This is possible in the clusters A496 and A133, for which the projected temperature profiles are also published [25, 29]. The resulting pressure profile are smoother due to the projection, but the pressure discontinuity, albeit reduced, is still seen.

To examine the sensitivity of the results to our two-point power-law fit, we examine a different fit procedure. Instead of using only the two nearest data points on each side of the CF, we include all points of radius within a factor 2 from the CF. We avoid any additional CF, so a single power-law may still provide a good approximation. All results change within their computed error bars, with a slight tendency towards  $\xi$  values closer to, but still smaller than, unity. The average in this case increases, due to the smoothing effect of the fit, to  $\bar{\xi} = 0.85 \pm 0.04$ .

As a general test against possible systematic errors (including the above deprojection and fit errors), we compute  $\xi$  with the same data and in the same method used to produce Figure 1, but for radii where no CF is present. This is possible in five CC sectors, in which we place a fictitious CF between every two consecutive radial bins away from the true CFs. The resulting  $\xi$  values, shown in Figure 2, lie above the CF mean of Eq. (1) for all but two fictitious CFs (both in the narrow sector in Virgo, excluded from the above analysis due to suspected density substructure). The mean value here is  $\bar{\xi} = 1.05 \pm 0.03$ ; without Virgo it becomes  $\bar{\xi} = 1.03 \pm 0.06$ . We similarly analyze the deprojected, azimuthally-averaged radial profiles (from [32–34]), which are sensitive to some systematic errors [50]. This gives  $\bar{\xi} = 1.04 \pm 0.01$ .

We conclude that there are small but significant drops in  $P_{th}$  below CFs, given on average by Eq. (1). None of the systematic effects considered can mimic this result.

*The missing pressure is nonthermal.*— A drop in the total pressure below the CF would imply some radial motion, perpendicular to the CF surface. As the flow must parallel the tangential discontinuity, such a drop would correspond to inward acceleration of the CF, or outward ram pressure of the gas below the CF [1]. However, a 20% pressure jump would correspond [13] to Mach  $\mathcal{M} \simeq 0.5$  radial motion: unrealistic in an otherwise relaxed core. Moreover, core CFs are thought to be part of extended three-dimensional surfaces spanning much of the core, so the implied coherent radial motion is unlikely.

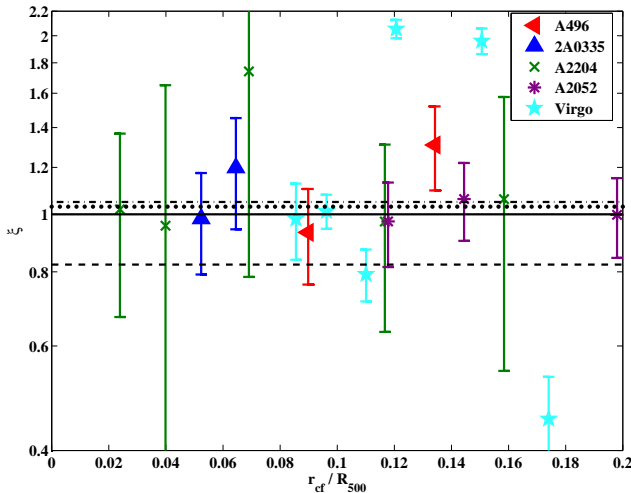


FIG. 2: Fictitious CFs. Horizontal  $\xi > 1$  lines show the averages  $\xi$  of these CFs, with (dotted) and without (dot-dashed) Virgo. The other lines are defined in Figure 1.

Hence, the total pressure must be nearly continuous across the CF, so the missing pressure must arise from some nonthermal component. The pressure drop we find imposes a lower limit on the nonthermal pressure  $P_{nt}$  below the CF, as our measurement is not sensitive to any additional, smoothly varying nonthermal component.

There is prior evidence for nonthermal pressure in clusters. Comparing optical and X-ray data gives  $\eta_{nt} \equiv P_{nt}/P_{th} \lesssim 10\%$  in the cores of Virgo and Fornax [35]. Comparing X-ray and weak lensing data yields  $\eta_{nt} \sim 30\%$  in MS2137 [36]. However, these estimates assume hydrostatic equilibrium, and are not specific to CFs.

*The distribution of nonthermal pressure.*— To further investigate the nature of  $P_{nt}$ , we compare the deprojected  $P_{th}$  profiles of several CF sectors with the azimuthally-averaged deprojected profiles of their host clusters. This can be done for A2204, A496, 2A0335, and Virgo, as shown in Figure 3. The radial means of the latter three clusters [32, 34] were published separately from the CF analyses; we divide their  $P_{th}$  by a fudge factor  $\sim 1.7$  of an unknown origin in order to match the CF sectors away from the CFs; this normalization has no effect on the results above. Also shown are the extrapolated  $P_{th}(r_{cf})$ , assuming power-law pressure profiles. The pressure discontinuities at the CFs are marked by rectangles.

Figure 3 suggests that in Virgo and in the inner CF of 2A0335,  $P_{th}$  above the CF is comparable to the mean pressure at that radius, whereas below the CF,  $P_{th}$  (circles) drops below its mean value (squares). The pressure deviation is confined to the narrow region  $\sim [0.7, 1]r_{cf}$ . This roughly corresponds to the shear flow layer [6, 11], suggesting that  $P_{nt}$  is associated with shear.

However, in A2204 and possibly in A496,  $P_{th}$  in the CF sector deviates predominately *above* the azimuthal

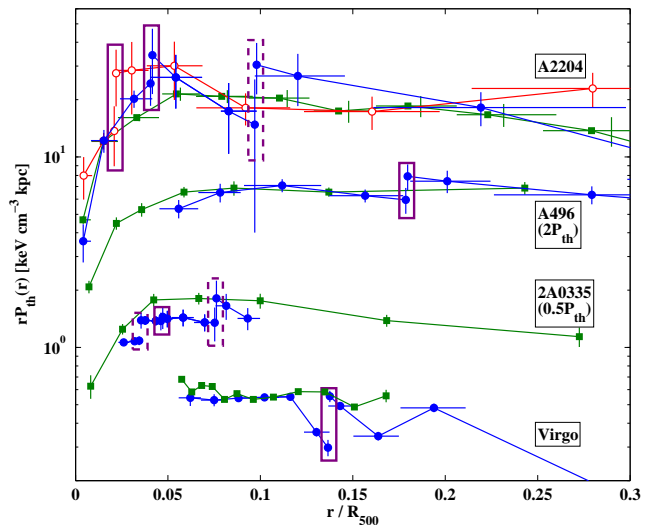


FIG. 3: Deprojected  $P_{th}$  profiles in CF sectors (circles, empty red or filled blue) and in their host clusters on average (green squares), multiplied by  $r$  to highlight the CFs. Connecting lines are guides to the eye. CFs are marked by rectangles (dashed for the new CFs, in A2204 and 2A0335). For clarity,  $P_{th}$  is multiplied by a factor of 2 in A496, and by 0.5 in 2A0335 (see labels). Data: The mean profiles of A496 and 2A0335 are from [32], Virgo from [34], and A2204 from averaging the four quadrants in [33]. The CF profiles for A2204 are from [24], A496 from [25], 2A0335 from [23] and Virgo from [31].

average just *above* the CF, and returns to the mean value slightly below the CF. The  $P_{th}$  deviations are roughly in the region  $[0.9, 1.5]r_{cf}$ , and are persistent although not highly significant. At face value, they suggest that while  $P_{nt}$  just below the CF is enhanced,  $P_{nt}$  just above these CFs is lower than typical of that radius. In such clusters, the nonthermal (and probably shear) layer may extend far beneath the CF, dominating much of the core.

However, a more detailed analysis is needed to reliably map  $P_{nt}(r)$ . The azimuthal averages used here are sensitive to normalization problems (although not in A2204), non-sphericity, and deprojection errors. In addition, the radial mean is biased by the CFs themselves, if the underlying high density layers are spatially extended as the data suggest. Here, the bright layer below a CF dominates the emission at that radius, and its enhanced  $P_{nt}$  may effectively lower the azimuthally averaged  $P_{th}$ .

*The nonthermal pressure is mostly magnetic.*— The CF phenomenology strongly constrains the nature of the nonthermal pressure, as the effect is (i) robust across different clusters; (ii) seen at various radii, both inside and outside the peak temperature radius; (iii) is mostly localized at CFs; and (iv) does not spread above the very narrow CF transitions. Shear-generated magnetic fields in the shear layers found beneath all CFs [11] naturally fulfill all these conditions. Three alternative explanations are considered in the discussion below: high-energy particles, small-scale turbulence (microturbulence), and

TABLE I: The most significantly nonzero magnetic fields below the CF, assuming  $\eta_B = \eta_{nt}$ , sorted by significance.

Cluster	$r_{cf}$ [kpc]	$\eta_B = 1 - \xi$	$B$ [ $\mu$ G]
A133	19	$0.31 \pm 0.08$	$33.6^{+4.3}_{-5.0}$
2A0335	29	$0.22 \pm 0.09$	$25.8^{+4.9}_{-6.0}$
A496	159	$0.25 \pm 0.13$	$15.3^{+3.6}_{-4.7}$
A2142	262	$0.22 \pm 0.13$	$21.9^{+4.8}_{-8.2}$
2A0335	62	$0.27 \pm 0.17$	$21.5^{+5.8}_{-8.3}$

a multiphase plasma. None of these are found to provide a viable explanation for the observations.

We conclude that the most natural, and the only self-consistent, interpretation of the nonthermal pressure is that it is predominantly, if not entirely, magnetic, in accordance with the CF-based motivation outlined above. Indeed, a predominantly magnetic  $\eta_{nt} = 1 - \xi \simeq 0.2$  can explain the stability of CFs [11, 37], the sharpness of the discontinuity, and the CF-minihalo connection. Our most significantly nonzero magnetic field measurements, assuming  $\eta_B = \eta_{nt}$ , are given in Table I.

The discontinuity in the magnetic field must be in the tangential component, as  $\nabla \cdot \mathbf{B} = 0$ , in accordance with the shear magnetization model [11]. Such strong fields are sufficiently strong to suppress the heat-flux buoyancy instability [38], which would otherwise tend to radially orient the magnetic field in the inner core.

*Discussion.*— By analyzing all 18 deprojected core CF profiles from the literature, including three newly identified CFs (Figure 3), we discover small but significant (see Eq. (1)) drops in  $P_{th}$  below the CFs. Such a discontinuity is seen in all non-merger CFs (Figure 1), while control samples (Figure 2) show no such trend; systematic effects are ruled out. The most natural interpretation is an enhanced nonthermal pressure, most likely magnetic, confined beneath the CF. Here, the nonthermal fraction reaches  $\eta_{nt} \simeq 20\%$  of equipartition; it declines inward but is still noticeable  $\sim 1/3$  and sometimes more (see Figure 3) of the distance towards the center of the cluster.

Such strong magnetization suffices to explain the CF-minihalo connection, stabilize the CF, and suppress transport across it, as needed to keep the discontinuity sharp. The strong magnetization, its sharp rise below the CF, and its coincidence with the shear layer, suggest saturated magnetic amplification by shear. Note that magnetic saturation at similar levels,  $\eta_B \sim 0.1$ , is sometimes inferred from observations of radio-bright regions in the ICM, in radio halos and relics [39]. The typical amplitudes of the magnetic field, demonstrated in Table I, broadly agree with Faraday rotation measurements [19] and minihalo estimates [17].

Although our results require a predominantly magnetic  $P_{nt}$  below the CF,  $\lesssim 1/2$  of the localized nonthermal pressure could have a different nature. Consider first a high-energy particle contribution to  $P_{nt}$ . Its pressure

fraction, estimated as  $\eta \simeq 10^{-3}$  in the centers of both cool-core [17] and merger [39, 40] clusters, is dynamically negligible. Shear acceleration [41] is too slow to be efficient in the ICM. AGN feedback is strongly diminished at  $r \gtrsim$  few 10 kpc CFs. In conclusion, a diffuse high-energy component is negligible at the CFs. AGN bubbles could significantly contribute to  $P_{nt}$ ; here, the associated magnetic component must be large.

Next, consider microturbulence. No direct measurement of turbulent pressure is presently available. Upper limits on the projected velocity dispersion, at the level of  $\eta_{nt} < 5\text{--}20\%$ , were imposed in several clusters [35, 42–44]. However, the apparent CF stability and narrowness imply that microturbulence cannot dominate the local enhancement of  $P_{nt}$ . In particular, this strongly restricts the allowed level of *shear-induced* microturbulence. Here,  $P_B$  at least as strong as the turbulent pressure is required in order to prevent the turbulent flow from broadening and disrupting the CF. However, such strong,  $\eta_B \gtrsim 0.1$  magnetization would stabilize the KHI, thus preventing the growth of turbulence in the first place.

Deviations from a single phase ideal gas can produce erroneous pressure profiles, rendering our fit inappropriate (*e.g.*, [25]). Such effects are unlikely to significantly distort our results, as this would require the same type of error over a non-negligible range of temperatures, a wide range of densities, and in the different environments inside and outside the temperature peak. Moreover, recent work shows that (i) the (projected) temperature jump across CFs is *larger* (by  $\sim 10\%$ ) in a multiphase model [45]; and (ii) X-ray observations of CCs are consistent at any given position with a single plasma phase [46]. Finally, note that different multiphase plasmas on each side of the CF would still require strong magnetization, to stabilize the CF and isolate the plasma.

This research has received funding from the European Union Seventh Framework Programme (FP7/2007-2013) under grant agreement n° 293975.

---

\* Electronic address: reissi@post.bgu.ac.il

- [1] M. Markevitch and A. Vikhlinin, Phys. Rep. **443**, 1 (2007), arXiv:astro-ph/0701821.
- [2] Y. Birnboim, U. Keshet, and L. Hernquist, MNRAS **408**, 199 (2010), 1006.1892.
- [3] M. Markevitch, A. Vikhlinin, and W. R. Forman, in *Astronomical Society of the Pacific Conference Series*, edited by S. Bowyer and C.-Y. Hwang (2003), vol. 301, p. 37, arXiv:astro-ph/0208208.
- [4] M. S. Owers, P. E. J. Nulsen, W. J. Couch, and M. Markevitch, ApJ **704**, 1349 (2009), 0909.2645.
- [5] Y. Ascasibar and M. Markevitch, ApJ **650**, 102 (2006), arXiv:astro-ph/0603246.
- [6] U. Keshet, ApJ **753**, 120 (2012), 1111.2337.
- [7] M. Markevitch, A. Vikhlinin, and P. Mazzotta, ApJ **562**, L153 (2001), arXiv:astro-ph/0108520.

- [8] E. R. Tittley and M. Henriksen, *ApJ* **618**, 227 (2005), arXiv:astro-ph/0409177.
- [9] E. Churazov, W. Forman, C. Jones, and H. Böhringer, *ApJ* **590**, 225 (2003), arXiv:astro-ph/0301482.
- [10] Y. Fujita, T. Matsumoto, and K. Wada, *ApJ* **612**, L9 (2004), arXiv:astro-ph/0407368.
- [11] U. Keshet, M. Markevitch, Y. Birnboim, and A. Loeb, *ApJ* **719**, L74 (2010), 0912.3526.
- [12] J. A. ZuHone, M. Markevitch, and D. Lee, *ApJ* **743**, 16 (2011), 1108.4427.
- [13] A. Vikhlinin, M. Markevitch, and S. S. Murray, *ApJ* **551**, 160 (2001), arXiv:astro-ph/0008496.
- [14] P. Mazzotta and S. Giacintucci, *ApJ* **675**, L9 (2008), 0801.1905.
- [15] S. Giacintucci, M. Markevitch, G. Brunetti, R. Cassano, and T. Venturi, *A&A* **525**, L10 (2011), 1011.3141.
- [16] J. ZuHone, M. Markevitch, G. Brunetti, and S. Giacintucci, *ArXiv e-prints* (2012), 1203.2994.
- [17] U. Keshet and A. Loeb, *ApJ* **722**, 737 (2010), 1003.1133.
- [18] C. L. Carilli and G. B. Taylor, *ARA&A* **40**, 319 (2002), arXiv:astro-ph/0110655.
- [19] T. E. Clarke, *Journal of Korean Astronomical Society* **37**, 337 (2004), arXiv:astro-ph/0412268.
- [20] F. Govoni, K. Dolag, M. Murgia, L. Feretti, S. Schindler, G. Giovannini, W. Boschin, V. Vacca, and A. Bonafede, *A&A* **522**, A105 (2010), 1007.5207.
- [21] A. Bonafede, F. Govoni, L. Feretti, M. Murgia, G. Giovannini, and M. Brüggen, *A&A* **530**, A24 (2011).
- [22] T. H. Reiprich and H. Böhringer, *ApJ* **567**, 716 (2002), arXiv:astro-ph/0111285.
- [23] J. S. Sanders, A. C. Fabian, and G. B. Taylor, *MNRAS* **396**, 1449 (2009), 0904.1374.
- [24] J. S. Sanders, A. C. Fabian, and G. B. Taylor, *MNRAS* **356**, 1022 (2005), arXiv:astro-ph/0406094.
- [25] T. Tanaka, H. Kunieda, M. Hudaverdi, A. Furuzawa, and Y. Tawara, *PASJ* **58**, 703 (2006).
- [26] M. Markevitch, T. J. Ponman, P. E. J. Nulsen, M. W. Bautz, D. J. Burke, L. P. David, D. Davis, R. H. Donnelly, W. R. Forman, C. Jones, et al., *ApJ* **541**, 542 (2000), arXiv:astro-ph/0001269.
- [27] J. de Plaa, N. Werner, A. Simionescu, J. S. Kaastra, Y. G. Grange, and J. Vink, *A&A* **523**, A81 (2010), 1008.3109.
- [28] R. E. Johnson, M. Markevitch, G. A. Wegner, C. Jones, and W. R. Forman, *ApJ* **710**, 1776 (2010), 1001.2441.
- [29] S. W. Randall, T. E. Clarke, P. E. J. Nulsen, M. S. Owers, C. L. Sarazin, W. R. Forman, and S. S. Murray, *ApJ* **722**, 825 (2010), 1008.2921.
- [30] R. E. Johnson, J. ZuHone, C. Jones, W. R. Forman, and M. Markevitch, *ApJ* **751**, 95 (2012), 1106.3489.
- [31] O. Urban, N. Werner, A. Simionescu, S. W. Allen, and H. Böhringer, *MNRAS* **414**, 2101 (2011), 1102.2430.
- [32] T. Tamura, J. S. Kaastra, J. A. M. Bleeker, and J. R. Peterson, in *Workshop on Galaxies and Clusters of Galaxies* (2003), p. 65.
- [33] J. S. Sanders, A. C. Fabian, and G. B. Taylor, *MNRAS* **393**, 71 (2009), 0811.0743.
- [34] E. Roediger, M. Brüggen, A. Simionescu, H. Böhringer, E. Churazov, and W. R. Forman, *MNRAS* **413**, 2057 (2011), 1007.4209.
- [35] E. Churazov, W. Forman, A. Vikhlinin, S. Tremaine, O. Gerhard, and C. Jones, *MNRAS* **388**, 1062 (2008), 0711.4686.
- [36] I. Chiu, S. M. Molnar, and P. Chen, *ArXiv e-prints* (2012), 1206.0532.
- [37] A. A. Vikhlinin and M. L. Markevitch, *Astronomy Letters* **28**, 495 (2002), arXiv:astro-ph/0209551.
- [38] E. Quataert, *ApJ* **673**, 758 (2008), 0710.5521.
- [39] U. Keshet, *ArXiv e-prints* (2010), 1011.0729.
- [40] D. Kushnir, B. Katz, and E. Waxman, *J. Cosmology Astropart. Phys.* **9**, 24 (2009), 0903.2275.
- [41] F. M. Rieger and P. Duffy, *ApJ* **652**, 1044 (2006), arXiv:astro-ph/0610187.
- [42] J. S. Sanders, A. C. Fabian, R. K. Smith, and J. R. Peterson, *MNRAS* **402**, L11 (2010), 0911.0763.
- [43] J. S. Sanders, A. C. Fabian, and R. K. Smith, *MNRAS* **410**, 1797 (2011), 1008.3500.
- [44] G. E. Bulbul, R. K. Smith, A. Foster, J. Cottam, M. Loewenstein, R. Mushotzky, and R. Shafer, *ApJ* **747**, 32 (2012), 1110.4422.
- [45] S. Ghizzardi, S. De Grandi, and S. Molendi, in *Galaxy Clusters as Giant Cosmic Laboratories, Proceedings of a workshop held 21-23 May 2012 in Madrid, Spain. Organized by the XMM-Newton Science Operations Centre of the European Space Agency (ESA).*, p.16, edited by J.-U. Ness (2012), p. 16.
- [46] S. Molendi and F. Pizzolato, *ApJ* **560**, 194 (2001), arXiv:astro-ph/0106552.
- [47] Planck Collaboration, P. A. R. Ade, N. Aghanim, M. Arnaud, M. Ashdown, F. Atrio-Barandela, J. Aumont, C. Baccigalupi, A. Balbi, A. J. Banday, et al., *ArXiv e-prints* (2012), 1207.4061.
- [48] A. Vikhlinin, A. Kravtsov, W. Forman, C. Jones, M. Markevitch, S. S. Murray, and L. Van Speybroeck, *ApJ* **640**, 691 (2006), arXiv:astro-ph/0507092.
- [49] Although some uncertainties are log-normal distributed.
- [50] Induced, for example, by a negative third derivative of  $\log(P)$  with respect to  $\log(r)$ , as found in the total CC pressure [47], and in the gas pressure at small radii [48].